Circular scanning fluorescence correlation spectroscopy on membranes

Zdeněk Petrášek[1,*], **Susan Derenko**[1] **and Petra Schwille**[1]

[1] *Biotechnologisches Zentrum, Technische Universität Dresden, Tatzberg 47/49, 01307 Dresden, Germany*

[*] *zdenek.petrasek@biotec.tu-dresden.de*

Abstract: We discuss circular scanning Fluorescence Correlation Spectroscopy (sFCS) as a simple extension of standard FCS for accurate, robust and fast diffusion measurements on membranes. The implementation is based on a straightforward conversion of a conventional FCS instrument to a sFCS device by mounting a mirror onto a two-axis piezo scanner. The measurement volume is scanned in a circle with sub-micron radius, allowing the determination of diffusion coefficients and concentrations without any a priori knowledge of the size of the detection volume. This is highly important in measurements on two-dimensional surfaces, where the volume size, and therefore the quantitative outcome of the experiment, is determined by the relative position of the surface and the objective focus, a parameter difficult to control in practice. The technique is applied to diffusion measurements on model membrane systems: supported lipid bilayers and giant unilamellar vesicles. We show that the method is insensitive to membrane positioning and to disturbing processes on faster or slower time scales than diffusion, and yields accurate results even for fluctuating or drifting membranes. Its robustness, short measurement times, and small size of the probed area makes this technique particularly attractive for analyzing the properties of membranes and molecules diffusing and interacting within them.

OCIS codes: (180.2520) Fluorescence microscopy; (180.1790) Confocal microscopy; (290.1990) Diffusion; (240.6648) Surface dynamics; (040.3780) Low light level

References and links

1. E. L. Elson and D. Magde, "Fluorescence correlation spectroscopy. I. Conceptual basis and theory," Biopolymers **13**, 1–27 (1974).
2. R. Rigler and E. S. Elson, eds., *Fluorescence Correlation Spectroscopy. Theory and Application*, Chemical Physics Series (Springer Verlag, Berlin, 2001), 1st ed.
3. K. Bacia and P. Schwille, "A dynamic view of cellular processes by in vivo fluorescence auto- and cross-correlation spectroscopy," Methods **29**, 74–85 (2003).
4. D. Axelrod, D. E. Koppel, J. Schlessinger, E. Elson, and W. W. Webb, "Mobility measurement by analysis of fluorescence photobleaching recovery kinetics," Biophys. J. **16**, 1055–1069 (1976).
5. M. J. Saxton and K. Jacobson, "Single-particle tracking: Applications to membrane dynamics," Annu. Rev. Biophys. Biomol. Struct. **26**, 373–399 (1997).
6. A. J. García-Sáez and P. Schwille, "Fluorescence correlation spectroscopy for the study of membrane dynamics and protein/lipid interactions," Methods **46**, 116–122 (2008).
7. R. Macháň and M. Hof, "Lipid diffusion in planar membranes investigated by fluorescence correlation spectroscopy," Biochim. Biophys. Acta Biomembr. **1798**, 1377–1391 (2010).

#153144 - $15.00 USD Received 18 Aug 2011; revised 29 Sep 2011; accepted 1 Oct 2011; published 22 Nov 2011

8. P. Schwille, F. J. Meyer-Almes, and R. Rigler, "Dual-color fluorescence cross-correlation spectroscopy for multicomponent diffusional analysis in solution," Biophys. J. **72**, 1878–1886 (1997).
9. K. Bacia, S. A. Kim, and P. Schwille, "Fluorescence cross-correlation spectroscopy in living cells," Nat. Methods **3**, 83–89 (2006).
10. J. Enderlein, I. Gregor, D. Patra, and J. Fitter, "Art and artefacts of fluorescence correlation spectroscopy," Curr. Pharm. Biotechnol. **5**, 155–161 (2004).
11. S. Milon, R. Hovius, H. Vogel, and T. Wohland, "Factors influencing fluorescence correlation spectroscopy measurements on membranes: simulations and experiments," Chem. Phys. **288**, 171–186 (2003).
12. A. Benda, M. Beneš, V. Mareček, A. Lhotský, W. T. Hermens, and M. Hof, "How to determine diffusion coefficients in planar phospholipid systems by confocal fluorescence correlation spectroscopy," Langmuir **19**, 4120–4126 (2003).
13. E. Gielen, M. Vandeven, A. Margineanu, P. Dedecker, M. Van der Auweraer, Y. Engelborghs, J. Hofkens, and M. Ameloot, "On the use of z-scan fluorescence correlation experiments on giant unilamellar vesicles," Chem. Phys. Lett. **469**, 110–114 (2009).
14. T. Dertinger, V. Pacheco, I. von der Hocht, R. Hartmann, I. Gregor, and J. Enderlein, "Two-focus fluorescence correlation spectroscopy: A new tool for accurate and absolute diffusion measements," ChemPhysChem **8**, 433–443 (2007).
15. Z. Petrášek, C. Hoege, A. Mashaghi, T. Ohrt, A. A. Hyman, and P. Schwille, "Characterization of protein dynamics in asymmetric cell division by scanning fluorescence correlation spectroscopy," Biophys. J. **95**, 5476–5486 (2008).
16. Z. Petrášek, C. Hoege, A. A. Hyman, and P. Schwille, "Two-photon fluorescence imaging and correlation analysis applied to protein dynamics in *C. elegans* embryo," Proc. SPIE **6860**, 68601L (2008).
17. J. Ries, S. Chiantia, and P. Schwille, "Accurate determination of membrane dynamics with line-scan FCS," Biophys. J. **96**, 1999–2008 (2009).
18. M. A. Digman, C. M. Brown, P. Sengupta, P. W. Wiseman, A. R. Horwitz, and E. Gratton, "Measuring fast dynamics in solutions and cells with a laser scanning microscope," Biophys. J. **89**, 1317–1327 (2005).
19. J. P. Skinner, Y. Chen, and J. D. Müller, "Position-sensitive scanning fluorescence correlation spectroscopy," Biophys. J. **89**, 1288–1301 (2005).
20. Z. Petrášek and P. Schwille, "Precise measurement of diffusion coefficients using scanning fluorescence correlation spectroscopy," Biophys. J. **94**, 1437–1448 (2008).
21. H. Qian and E. L. Elson, "Analysis of confocal laser-microscope optics for 3-D fluorescence correlation spectroscopy," Appl. Opt. **30**, 1185–1195 (1991).
22. S. T. Hess and W. W. Webb, "Focal volume optics and experimental artifacts in confocal fluorescence correlation spectroscopy," Biophys. J. **83**, 2300–2317 (2002).
23. M. Born and E. Wolf, *Principles of Optics* (Cambridge University Press, 1999), chap. 8, pp. 484–492, 7th ed.
24. K. M. Berland, P. T. C. So, Y. Chen, W. W. Mantulin, and E. Gratton, "Scanning two-photon fluctuation correlation spectroscopy: Particle counting measurements for detection of molecular aggregation," Biophys. J. **71**, 410–420 (1996).
25. J. Widengren, U. Mets, and R. Rigler, "Fluorescence correlation spectroscopy of triplet states in solution: A theoretical and experimental study," J. Phys. Chem. **99**, 13368–13379 (1995).
26. S. Chiantia, N. Kahya, and P. Schwille, "Dehydration damage of domain-exhibiting supported bilayers: An AFM study on the protective effects of disaccharides and other stabilizing substances," Langmuir **21**, 6317–6323 (2005).
27. D. C. Carrer, E. Kummer, G. Chwastek, S. Chiantia, and P. Schwille, "Asymmetry determines the effects of natural ceramides on model membranes," Soft Matter **5**, 3279–3286 (2009).
28. N. Kahya, "Protein-protein and protein-lipid interactions in domain-assembly: Lessons from giant unilamellar vesicles," Biochim. Biophys. Acta Biomembr. **1798**, 1392–1398 (2010).
29. K. Bacia, D. Scherfeld, N. Kahya, and P. Schwille, "Fluorescence correlation spectroscopy relates rafts in model and native membranes," Biophys. J. **87**, 1034–1043 (2004).
30. M. Przybylo, J. Sýkora, J. Humpolíčková, A. Benda, A. Zan, and M. Hof, "Lipid diffusion in giant unilamellar vesicles is more than 2 times faster than in supported phospholipid bilayers under identical conditions," Langmuir **22**, 9096–9099 (2006).
31. S. Chiantia, J. Ries, N. Kahya, and P. Schwille, "Combined AFM and two-focus SFCS study of raft-exhibiting model membranes," ChemPhysChem **7**, 2409–2418 (2006).
32. U. Haupts, S. Maiti, P. Schwille, and W. W. Webb, "Dynamics of fluorescence fluctuations in green fluorescent protein observed by fluorescence correlation spectroscopy," Proc. Natl. Acad. Sci. U. S. A. **95**, 13573–13578 (1998).
33. J. Hendrix, C. Flors, P. Dedecker, J. Hofkens, and Y. Engelborghs, "Dark states in monomeric red fluorescent proteins studied by fluorescence correlation and single molecule spectroscopy," Biophys. J. **94**, 4103–4113 (2008).
34. J. Widengren and P. Schwille, "Characterization of photoinduced isomerization and back-isomerization of the cyanine dye Cy5 by fluorescence correlation spectroscopy," J. Phys. Chem. A **104**, 6416–6428 (2000).
35. K. Bacia and P. Schwille, "Practical guidelines for dual-color fluorescence cross-correlation spectroscopy," Na-

#153144 - $15.00 USD Received 18 Aug 2011; revised 29 Sep 2011; accepted 1 Oct 2011; published 22 Nov 2011

ture Protocols **2**, 2842–2856 (2007).
36. E. P. Petrov and P. Schwille, "Fluorescence correlation spectroscopy on undulating membranes," Biophys. J. **88**, 524A–525A (2005).
37. J. Evans, W. Gratzer, N. Mohandas, K. Parker, and J. Sleep, "Fluctuations of the red blood cell membrane: Relation to mechanical properties and lack of ATP dependence," Biophys. J. **94**, 4134–4144 (2008).
38. M. B. Schneider, J. T. Jenkins, and W. W. Webb, "Thermal fluctuations of large quasi-spherical bimolecular phospholipid-vesicles," Journal De Physique **45**, 1457–1472 (1984).
39. Y. Korlann, T. Dertinger, X. Michalet, S. Weiss, and J. Enderlein, "Measuring diffusion with polarization-modulation dual-focus fluorescence correlation spectroscopy," Opt. Express **16**, 14609–14616 (2008).
40. P. Ferrand, M. Pianta, A. Kress, A. Aillaud, H. Rigneault, and D. Marguet, "A versatile dual spot laser scanning confocal microscopy system for advanced fluorescence correlation spectroscopy analysis in living cell," Rev. Sci. Instrum. **80**, 083702 (2009).
41. C. Eggeling, C. Ringemann, R. Medda, G. Schwarzmann, K. Sandhoff, S. Polyakova, V. N. Belov, B. Hein, C. von Middendorff, A. Schönle, and S. W. Hell, "Direct observation of the nanoscale dynamics of membrane lipids in a living cell," Nature **457**, 1159–1162 (2009).

1. Introduction

The ability to experimentally quantify transport properties and concentrations of molecules on microscopic scales, both in three dimensions and when confined to surfaces, such as cellular membranes, is essential for understanding the details of biological processes on molecular level. The membranes have not only the obvious function of separating different compartments and controlling material exchange between them, but they themselves constitute an environment where biochemical reactions take place. Experimental approaches probing the properties of membranes and molecules interacting with them are therefore of great relevance.

Several optical methods for investigating molecular transport that are readily combined with fluorescence imaging are available: Fluorescence Correlation Spectroscopy (FCS) [1–3], Fluorescence Recovery After Photobleaching (FRAP) [4] and Single Particle Tracking (SPT) [5]. FCS has several advantages over the other methods, most importantly: the measurement is performed within very small (sub-μm) volume, allowing for high spatial resolution; high temporal resolution, sufficient practically for any biologically relevant molecular transport process; and the ability to determine concentrations by quantifying the magnitude of fluorescence fluctuations without having to rely on the knowledge of molecular brightness. FCS is often applied to the investigation of molecular diffusion in planar membrane systems [6, 7]. Molecular interactions can be monitored by extending FCS to use two excitation and emission channels and two distinct fluorescent labels: Fluorescence Cross-Correlation Spectroscopy (FCCS) [8, 9].

One difficulty in obtaining accurate values of both diffusion coefficients and concentrations with FCS is the need to know the size of the volume in which the measurement takes place. The volume size is usually determined by calibration using a well defined standard sample. However, the differences in the volume size between the calibration and the actual measurement lead to errors [10]. For measurements in bulk (3D), the possible deviations from the calibration value are caused by optical distortions of the diffraction-limited beam. The situation in two dimensions is more complicated: the measurement volume, or rather the area, is defined by the cross-section of the plane with the 3D volume formed by a combined effect of focused laser beam and the confocal pinhole. The relative position of the two defines the size of the volume, therefore the uncertainty about the volume size remains even in the absence of optical distortions [11, 12].

The ideal axial volume position, with the membrane in the objective focal plane, is difficult to adjust experimentally, because of a rather weak dependence of the fluorescence intensity on the axial position of the surface to which the molecules are confined, and also because in practice the position of the maximum of fluorescence intensity does not necessarily coincide with the focal waist [12].

#153144 - $15.00 USD Received 18 Aug 2011; revised 29 Sep 2011; accepted 1 Oct 2011; published 22 Nov 2011

One solution to the positioning problem in membrane experiments is to perform a series of measurements at a range of axial positions and analyze these globally while making an assumption about the shape of the 3D profile of the focused laser beam: the z-scan method [12]. The drawback of this approach is the need to do many measurements, requiring a considerable time, which calls for a high axial stability of the sample on a sub-μm scale. Additionally, even though every single measurement is limited to a plane, the method relies on the assumption of a well-defined volume shape in three dimensions [12, 13].

Another way to deal with the volume problem is to avoid the need for independent volume calibration by employing spatio-temporal correlation techniques. These methods measure and analyze fluorescence correlations between two or more spatially distinct locations, rather than analyzing temporal correlations at a single position. The principle is based on the fact, that the distances between these locations, which can be determined independently of the actual experiment with sufficient accuracy, and are not affected by the optical properties of the sample, provide the required spatial reference scale, as an alternative to the volume size in standard FCS. Examples of these spatio-temporal extensions of FCS include: double-focus FCS [14], scanning FCS (sFCS) with a large circle [15, 16] or a line [17], raster scan FCS (RICS) [18], and small-circle sFCS [19, 20].

Here we present a new simple implementation of small-circle sFCS. It is realized as an easy extension of an existing FCS setup by replacing a mirror with a two-axis piezo scanner, and, contrary to our previous version implemented within a two-photon microscope [20], uses one-photon excitation with the advantages of simpler implementation and better signal-to-noise ratios. The method is applied to diffusion measurements of molecules in model membrane systems: supported lipid bilayers (SLB) and giant unilamellar vesicles (GUV). We show that the this type of sFCS on membranes does not suffer from the axial positioning problem, and is highly precise and robust with respect to undesirable effects that may strongly disturb conventional FCS measurements, such as sample drift or membrane thermal fluctuations.

2. Theory

The shape of the volume from within which the fluorescence is measured in a FCS experiment is determined by a combination of the illumination and the detection profiles [21, 22]. The light intensity near the focus of a high-NA lens is described by a complex diffraction pattern [23]; the detection efficiency is additionally determined by the confocal pinhole [22]. The combined effect of confinement due to illumination and detection is for the purpose of FCS usually approximated by a three-dimensional Gaussian function [2] or, more accurately, by a function where the illumination component $W_{\mathrm{ex}}(\mathbf{r})$ has the form of a Gaussian-Lorentzian function [14]:

$$W_{\mathrm{ex}}(\mathbf{r}) = \frac{a_0^2}{a^2(z)} e^{-\frac{x^2+y^2}{2a^2(z)}}, \tag{1}$$

where the lateral volume extent a depends on the axial distance z from the focal plane in the following way:

$$a^2(z) = a_0^2 + b^2 z^2, \quad b = \frac{\lambda}{4\pi n a_0}, \tag{2}$$

where λ is the excitation wavelength, n the refractive index of the medium, and a_0 the volume size in the focal plane. The value of a_0 is determined by the wavelength and the NA of illumination.

When measuring fluorescence of molecules restricted to a horizontal plane, the illuminated area, playing the same role as the measurement volume in 3D, is defined by a cross-section

#153144 - $15.00 USD Received 18 Aug 2011; revised 29 Sep 2011; accepted 1 Oct 2011; published 22 Nov 2011

of the 3D illuminated volume (Eq. (1)) with the plane, and is therefore described by a simple Gaussian function.

Equation (2) forms the basis of the z-scan method for reliable determination of diffusion coefficients in plane [12]. In this method, the diffusion coefficient D and a_0 are obtained from a fit to an experimental dependence of the diffusion time $\tau_D(z) = a^2(z)/D$ on the axial position z of the membrane within the focus. For this purpose, a series of autocorrelation curves at well defined axial positions has to be measured. The method relies on the validity of Eq. (2), namely the dependence of the volume size a on z, and the dependence of the parameter b, the axial beam divergence near the focus, on the wavelength and a_0.

In sFCS performed in 2D, we also assume that the cross-section of the laser beam with the plane can be approximated by a Gaussian, however, do not make any assumptions on how the width a of this Gaussian depends on z (Eq. (3)):

$$W(x,y) = e^{-\frac{x^2+y^2}{2a^2}}. \tag{3}$$

The uniform motion of the measurement volume in a circle with a radius R and frequency f modifies the model fluorescence autocorrelation function for diffusion restricted to two dimensions by an additional exponential factor, yielding [19, 20, 24]:

$$g(\tau) = \frac{1}{cV_{eff}} \frac{1}{1+\frac{\tau}{\tau_D}} e^{-\frac{R^2 \sin^2(\pi f \tau)}{a^2\left(1+\frac{\tau}{\tau_D}\right)}}, \tag{4}$$

where V_{eff} is the effective measurement volume (area), $V_{eff} = 4\pi a^2$, and τ_D the diffusion time:

$$\tau_D = a^2/D. \tag{5}$$

The sFCS autocorrelation exhibits periodic modulation due to the circular motion of the volume. The maxima, the minima and the width of the correlation peaks depend on the diffusion coefficient D and volume size a in an independent way, making it possible to determine both these parameters from a fit to Eq. (4), as schematically shown in Fig. 1 and described earlier [20].

When the membrane coincides with the objective focal plane (Fig. 1(A), left), the illuminated area is the smallest possible (low a), and there is minimal overlap between the focus positions separated by the largest possible distance — the scan circle diameter $2R$. When the membrane is moved out of focus, the illuminated area becomes larger (higher a) and so does the overlap between two positions separated by $2R$. This leads not only to the decrease of the autocorrelation amplitude and an increase in the diffusion time, as in standard FCS, but affects the shape of the autocorrelation in a complex way, for example, the value at the first minimum at $\tau = 1/(2f)$ increases due to the larger overlap when off focus (Fig. 1(B)). Since these changes, caused by an increase of a, are different from the changes that would be caused by variations in the diffusion coefficient, the diffusion coefficient and the volume size can be obtained simultaneously from the fit of a single experimental sFCS autocorrelation to Eq. (4), unlike in standard FCS, which yields only their combination in form of the diffusion time τ_D.

The uncorrelated character of D and a is apparent from the contour plot of χ_r^2 in the parameter space of D and a, constructed by fitting an experimental curve with a model with fixed values of D and a (Fig. 1(C)). Not only does the plot exhibit a clear single minimum with respect to D and a, but additionally the minimum of χ_r^2 with respect to D is practically independent of a for any fixed value of a near the absolute minimum, and vice versa, meaning that the two parameters are not correlated.

This is in contrast to standard FCS, where the minimum of the χ_r^2 plot has a shape of an almost diagonal line, meaning that D and a are fully correlated. For every value of a a value of

#153144 - $15.00 USD Received 18 Aug 2011; revised 29 Sep 2011; accepted 1 Oct 2011; published 22 Nov 2011

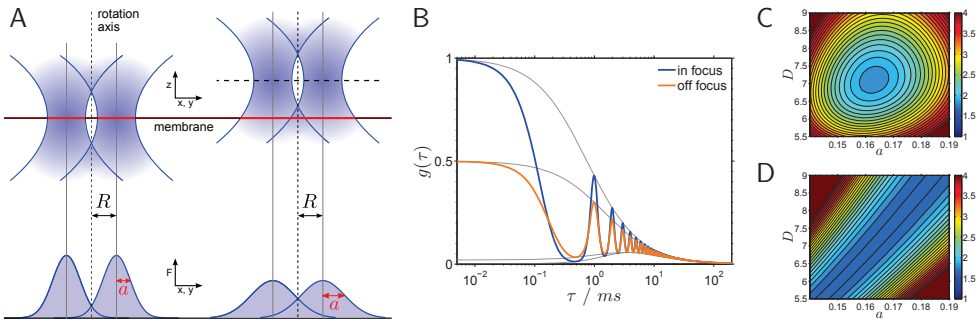

Fig. 1. The principle of circular scanning FCS on a 2D surface (membrane). A: The position of the objective focal plane with respect to the membrane plane affects not only the size a of the illuminated area on the membrane (the measurement volume V_{eff}), but also the volume (area) overlap between any two different beam positions (here shown for the maximum possible distance, the scan circle diameter $2R$). Left: the membrane coincides with the objective focus; Right: the membrane is below the objective focus. B: The axial displacement of the membrane away from the focus influences the autocorrelation in a complex way, changing not only the amplitude $g(0)$ and the diffusion time τ_D, but also affecting the shape of the correlation peaks. The distinct ways of how variations in D and a affect the correlation allows the determination of the diffusion coefficient D and the volume size a from a single autocorrelation curve. C: The χ_r^2 map as a function of D and a with a single minimum calculated from an experimental sFCS curve, demonstrating that D and a are uncorrelated. D: The χ_r^2 map for a standard FCS curve with a minimum for all values of D where $D = a^2/\tau_D$, showing that D and a are fully correlated.

D globally minimizing χ_r^2 exists, and vice versa, as determined by the combination of the two parameters in the diffusion time τ_D (Eq. (5), Fig. 1(D)).

The fact that the fit to sFCS data yields also the size of the illuminated area, parametrized by a, allows us to calculate the absolute surface concentration c of the diffusing molecules from the autocorrelation amplitude $g(0)$, using Eq. (4):

$$c = \frac{1}{g(0)V_{eff}} = \frac{1}{4\pi a^2 g(0)}. \tag{6}$$

The term accounting for triplet-induced fluctuations [25] was not included in the model, as the characteristic time of these fluctuations ($< 10\,\mu$s) is much shorter than the typical diffusion times of lipids and proteins in membranes (> 1 ms), and low excitation intensities were used, leading to low population of triplet states.

3. Materials and methods

3.1. *Experimental setup*

The experimental setup is almost identical with a standard FCS instrument (Fig. 2(A)): an expanded collimated laser beam fills the back aperture of the objective and is focused in the objective focal plane. The back-emitted fluorescence is collected and collimated by the same objective, reflected by a dichroic beamsplitter and focused onto an optical fibre, which serves as a confocal pinhole and guides the light to the detector. The scanning capability is achieved by replacing the last fixed mirror before the objective by a two-axis piezo scanner with a mounted circular mirror. Because of the short distance to the objective and small deflection angles, the

#153144 - $15.00 USD Received 18 Aug 2011; revised 29 Sep 2011; accepted 1 Oct 2011; published 22 Nov 2011

beam displacement on the back objective aperture is less than 0.1 mm and no additional relay lenses between the scanner and the objective are needed.

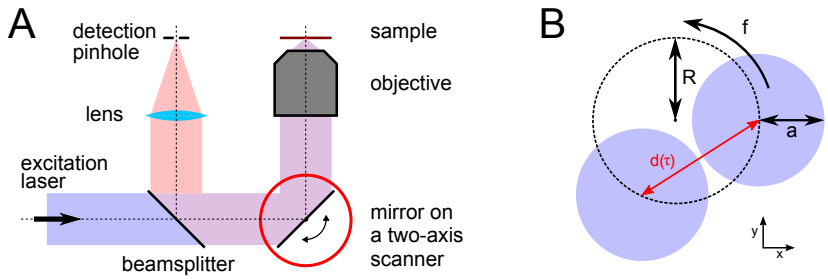

Fig. 2. The experimental setup for scanning FCS. A: The standard FCS setup is modified by mounting the last mirror before the back objective entry onto a two-axis piezo scanner. B: The scanner is used to move the beam uniformly, with a known frequency f, in a circle of radius R comparable to the size a of the focused beam. The distance d between two focus positions separated by a lag time τ varies between 0 and $2R$, and is uniquely determined by the relation $d = 2R\sin(\pi f \tau)$.

For excitation, a diode laser emitting at 488 nm (Sapphire 488-20, Coherent, Santa Clara, USA) was used. The emitted light was separated from the excitation by a beamsplitter with a reflection edge at 495 nm, and further passed through an emission filter 525/50 nm. The axial position of the objective (Olympus UPLAPO 60$\times$ W/IR) was controlled by a piezo objective scanner (P-721.10, PhysikInstrumente, Karlsruhe, Germany). The 100 μm-diameter optical fibre end functions as a rather large confocal pinhole, given the overall magnification of 53$\times$. The fluorescence was detected with an avalanche photodiode (APD) (SPCM-AQR, PerkinElmer, Waltham, Massachusetts, USA). The raw data (photoncount sequence with temporal resolution of 17 ns) were recorded with a correlator (Flex02-12D, Correlator.com, Bridgewater, USA) for further correlation analysis.

The scanning mirror was not synchronized with the fluorescence detection by the correlator, as synchronization is not necessary for the presented scanning FCS application. This simplifies the technical implementation of the method. Nevertheless, if required, synchronization can be realized by using a commonly available data acquisition card containing analog outputs for scanner control and counter inputs for fluorescence detection.

The two-axis piezo scanner (S-330.2SL, PhysikInstrumente, Karlsruhe, Germany) has a limited, but for our purpose fully sufficient, optical deflection range of 4 mrad. This translates to approx. 7.5 μm and 11 μm within the objective focal plane for the two axes. The factor of approx. $\sqrt{2}$ follows from the geometry of the optical path, where the beam hits the scanner mirror at 90°.

For the sFCS application an accurate calibration of the scan radius at the used frequency is very important. At low frequencies, where the scanner follows the driving signal, the calibration was performed by using the light reflected off a Ronchi ruling with 600 line pairs/mm, as described previously for galvano scanners [20]. At scan frequencies reaching and exceeding hundred Hz the scanner does not follow the driving signal exactly, resulting in reduced scan radii. The radius reduction factor was determined by comparing the signal from the accurate internal scanner position sensor at high and low frequencies. The radius reduction factors range from 0.9 at 50 Hz to 0.4 at 200 Hz. For the experiments described here the actual scanning radius R was 0.385 μm, the frequency f 200 Hz, and the measurement time 100 s.

#153144 - $15.00 USD Received 18 Aug 2011; revised 29 Sep 2011; accepted 1 Oct 2011; published 22 Nov 2011

The scanner was fully controlled via a LabView program. In addition to circular scans, a raster scan mode was programmed, allowing to obtain a small image ($7.5 \times 11\,\mu$m) of the sample and to select a suitable position for the sFCS measurement. For this purpose the signal from the APD was split between a correlator and a counter card (PCI-6602, National Instruments, Austin, Texas, USA) which was synchronized with the scanner and provided the pixel brightness values for the resulting image.

3.2. Data analysis

The autocorrelation functions were calculated from the raw data using the multiple-tau algorithm with increased resolution ($m = 64$), as described previously [20]. The data fitting was implemented in Matlab (Natic, USA); the model function was Eq. (4) with an additional offset parameter. The scan radius R and frequency f were always kept fixed to the known values, and the remaining parameters, D, a, the autocorrelation amplitude g_0 and an additive offset, were optimized by weighed nonlinear least-squares method (minimizing χ_r^2), with weights estimated from the data.

Non-uniformity of fluorescence along the scanned circle, caused, for example, by immobile bright objects located near one side of the scanned circle, can give rise to additional periodic pattern in the autocorrelation. This feature can be used to identify immobilized particles [19]. In our case these fluctuations were undesirable, and were therefore filtered out by a procedure described before [15]. In the majority of cases the non-uniformity in the data was very weak resulting in negligible difference when the filtering procedure was applied.

3.3. Sample preparation

The phospholipid 1,2-dioleoyl-*sn*-glycero-3-phosphocholine (DOPC) was purchased from Avanti Polar Lipids (Alabaster, USA), the dyes 3,3'-dioctadecyloxacarbocyanine perchlorate (DiO) and cholesteryl 4,4-difluoro-5,7-dimethyl-4-bora-3a,4a-diaza-*s*-indacene-3-dodecanoate (Bodipy-Chol) from Molecular Probes (Eugene, USA).

For the preparation of SLBs, chloroform solution of DOPC with 3×10^{-5} fraction of the dye was evaporated in a glass vial; then buffer (10 mM HEPES, 150 mM NaCl, pH=7.4) was added, the mixture was vortexed and sonicated until it became clear, resulting in a solution of small unilamellar vesicles (SUV). A small amount of the SUV solution was pipetted onto freshly cleaved mica attached to a coverslip, and $CaCl_2$ at final concentration of 3 mM was added, causing the SUVs to burst. After 30 min. of incubation the solution was gently washed multiple times, resulting in a single bilayer on the mica surface [26].

The GUVs were prepared by the electroformation method on Pt wires [27, 28]. The solution of DOPC in chloroform containing 5×10^{-5} Bodipy-Chol or DiO (3 μl) was pipetted onto Pt electrodes in a custom-made teflon chamber and the solvent was left to evaporate. Then the chamber was filled with 150 mM sucrose solution and voltage of 2 V at 10 Hz was applied for 30 min. to form GUVs. The GUVs were gently pipetted into 100 mM glucose solution in an observation chamber. The osmolarity difference tensed the GUVs and minimized the membrane thermal fluctuations; the difference in density of the inner and outer solutions made the GUVs sink to the bottom of the observation chamber. The preparation and measurements were done at the temperature 22°C.

4. Results

4.1. Independence on axial positioning

As discussed in the Theory section, the relative positioning of the horizontal membrane and the objective focus defines the measurement volume a (Fig. 1(A)), and consequently influences

#153144 - $15.00 USD Received 18 Aug 2011; revised 29 Sep 2011; accepted 1 Oct 2011; published 22 Nov 2011

the shape of the measured autocorrelation function (Fig. 1(B)). Nevertheless, the parameters of interest, the diffusion coefficient D and the concentration c of the diffusing molecules, should be obtained from the fits independently of the axial membrane position. In order to demonstrate this property of sFCS, we performed measurements on the top pole of a GUV (DOPC with DiO) at different axial membrane positions relative to the laser focus (Fig. 3).

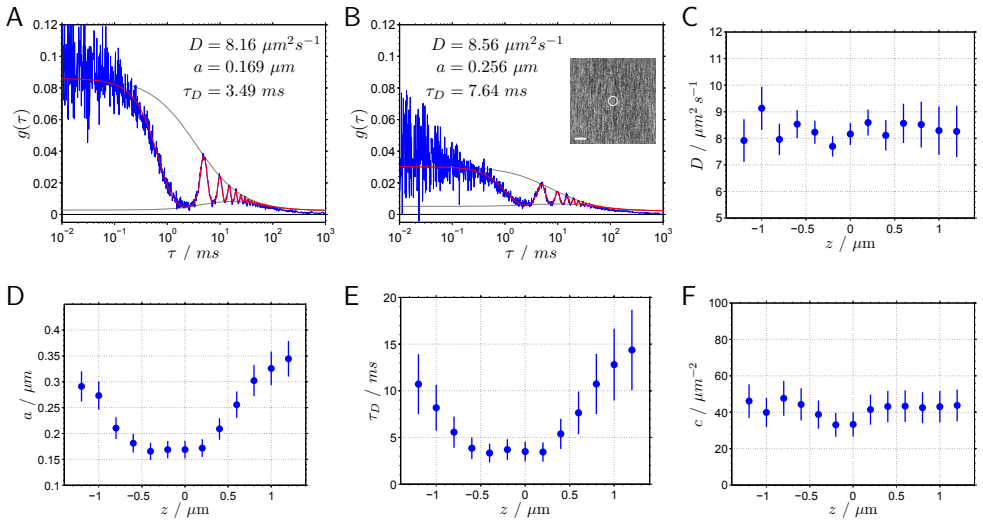

Fig. 3. The dependence of the autocorrelation curves and the fit parameters on the membrane position relative to the focal plane. The measurements with the membrane near the focal plane (A) and away from the focal plane (B) result in clearly different autocorrelations, with the fitting yielding different amplitudes $g(0)$, diffusion coefficients τ_D, and volume sizes a, but equal diffusion coefficients D. A series of measurements at different axial positions results in diffusion coefficient (C) and concentration (F) practically independent of the axial position, and the volume size (D) and diffusion time (E) exhibit a clear minimum when the membrane coincides with the objective focal plane. The inset in B shows the top pole of the GUV with the circular scan path (scale bar $1\,\mu$m). The sample was a GUV prepared with DOPC and DiO.

Figures 3(A) and (B) compare two autocorrelation curves measured at two different axial positions: with the membrane located near the objective focal plane (Fig. 3(A)), and displaced by approx. 0.6 μm away from the objective focus (Fig. 3(B)). As expected, the autocorrelation amplitude $g(0)$ is lower when out of focus, as the measurement area, therefore also the number of molecules within it, increases. Fitting the data confirms the increase of a and consequently also of the diffusion time τ_D, but, importantly, the diffusion coefficient does not change within the measurement precision.

Figures 3(C–F) summarize the results of a series of measurements at different axial positions where z varies in the range of 2.4 μm. The diffusion coefficient determined from the fits is practically independent of the axial position within the probed distance of $\pm 1.2\,\mu$m from the focal plane. As expected, the volume size a and the diffusion time τ_D exhibit a clear minimum, corresponding to the situation where the objective focal plane and the membrane position coincide.

The concentration calculated with Eq. (6) is also independent of the axial position (Fig. 3(F)), although the precision is lower than in the case of diffusion coefficient. In general, the experi-

#153144 - $15.00 USD Received 18 Aug 2011; revised 29 Sep 2011; accepted 1 Oct 2011; published 22 Nov 2011

ments performed on GUVs and SLBs show that the autocorrelation amplitude is more sensitive to the shape of the measurement volume.

A set of standard FCS measurement analogous to those in Fig. 3 would produce only diffusion times (as in Fig. 3(E)) which cannot be converted to diffusion coefficients without knowing a for each measurement. The diffusion times vary by a factor of four, which would under an assumption of a constant a transform into a large variation of D, also by a factor of four (Eq. (5)). When the axial displacement z is well controlled, the set of measurements in Fig. 3(E) can be analyzed by the z-scan method [12]. However, for the z-scan method to be applicable, a whole series of measurements at different and well defined axial positions is necessary. The major advantage of sFCS is that any single measurement at any axial position provides the diffusion coefficient.

A range of measurements performed on the same GUV or on the same position of SLB exhibited small variations, with standard deviation of D in a single measurement typically below 5%. However, the variations between different GUVs, or different positions on SLB, were larger, especially in case of SLBs. The diffusion coefficient of Bodipy-Chol in DOPC SLB was found in the range 3.1–4.1 μm^{2}s^{-1}, and of DiO in DOPC SLB 1.6–2.1 μm^{2}s^{-1}. Bodipy-Chol in GUVs made of DOPC diffused with D=7.8–9.3 μm^{2}s^{-1}, and DiO with D=6.7–8.5 μm^{2}s^{-1}. The exact reason for these variations, lying within 20–30%, is not known; a possible explanation for SLBs is the spatial variations of the interaction between the membrane and the support. The obtained values of D are in general agreement with previous reports [7, 13, 29–31].

In some situations, depending on the intensity of the washing step in the SLB preparation, patches of a second bilayer on the top of the continuous bilayer on mica were observed. The fluorescence intensity of these patches was twice that of the surrounding membrane, and the diffusion coefficient for Bodipy-Chol in DOPC SLB was 5.3–5.8 μm^{2}s^{-1}. This value represents an average of D in both bilayers, and, being closer to the diffusion coefficient in unsupported bilayer (GUV), suggests that the upper bilayer interacts much less with the support than the lower bilayer [30].

4.2. Fitting range

The key parameter obtained from a standard FCS experiment is the diffusion time τ_D, the time when when the autocorrelation $g(\tau)$ decreases to approximately one half of its initial value. In order to reliably determine this time from the data, the fitting time interval should be rather broad, covering at least a part of the curve close to its amplitude (short times) and the baseline (long times). This means a time interval at least two orders of magnitude wide.

The situation is different in sFCS, where the relative shapes of the peaks in the correlation function carry information about both the diffusion coefficient and the volume size, and a narrower fitting range is therefore sufficient. We investigated how a fitting range limited to a narrower interval (τ_1, τ_2) affects the values of the obtained diffusion coefficient (Fig. 4).

A set of 20 measurements on a SLB (DOPC with Bodipy-Chol) was analyzed in a range of intervals where either the initial part of the autocorrelation was excluded: the upper bound was fixed at $\tau_2 = 30$ ms and the lower bound ranged from 10 μs to 20 ms (Fig. 4(C)), or where the tail of the autocorrelation was ignored: the lower bound was fixed at $\tau_1 = 10\,\mu$s and the upper bound was varied from 5 ms to 300 ms (Fig. 4(D)).

In either case, the mean diffusion coefficient D and its variance are practically independent of both the width and the position of the fitting range. As Fig. 4(C) shows, even when the fitting range is as narrow as two periods of the scanner motion, from 10 ms to 30 ms, the diffusion coefficient and its variance are practically the same as when a much wider part of the autocorrelation is analyzed.

In order to compare the influence of the fitting range in scanning FCS with standard FCS, we

#153144 - $15.00 USD Received 18 Aug 2011; revised 29 Sep 2011; accepted 1 Oct 2011; published 22 Nov 2011

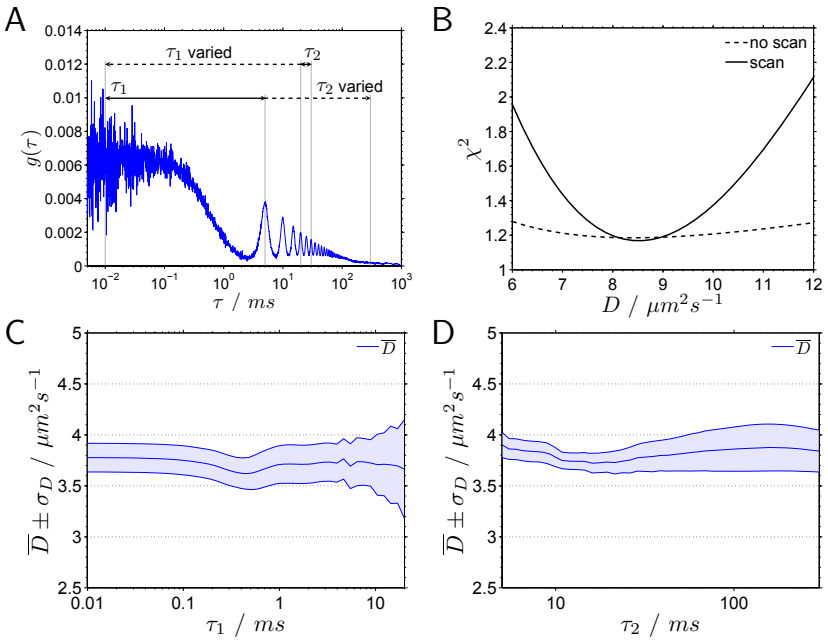

Fig. 4. The recovered diffusion coefficient is independent of the interval (τ_1, τ_2) in which the autocorrelation curve is analyzed. A: The range of intervals in which the data were analyzed had a variable lower bound τ_1 varying from 10 μs to 20 ms and the upper bound $\tau_2 = 30$ ms (C), or a fixed lower bound $\tau_1 = 10\,\mu$s and a variable upper bound varying from 5 ms to 300 ms (D). The mean diffusion coefficient $\overline{D}$ and its standard deviation σ_D calculated from 20 measurements are practically independent of the fitting range, both when the analysis is limited to either the short (C) or the longer (D) time scales. Sample: DOPC SLB with Bodipy-Chol. B: In circular scanning FCS, even a narrow fitting interval (2.5, 17.5) ms, that is, three scan periods, produces a deep, well defined minimum in χ^2_r, sufficiently restricting the diffusion coefficient (solid line). In standard FCS, the same narrow fitting interval leads to a very shallow minimum and is not sufficient to constrain D (dashed line). Sample: DOPC GUV with Bodipy-Chol.

looked at the depth of the χ^2_r minimum with respect to D. A deeper, more confined minimum of χ^2_r means that the fitting result is better defined and less susceptible to noise. Figure 4(B) shows the $\chi^2_r(D)$ profiles for measurements with and without scanning on a DOPC GUV with Bodipy-Chol. In both cases the fitting range was restricted to three scan periods, from 2.5 ms to 17.5 ms. The sFCS curve was fitted with a as a free parameter, the standard FCS curve was fitted with a fixed to 0.165 μm, a value returned from the sFCS fit at χ^2_r minimum. While the χ^2_r minimum of the sFCS data is well confined, allowing a robust fit, the minimum of the standard FCS data is very shallow, leading to a large spread of D values.

These results demonstrate an important advantage of circular sFCS over standard FCS: the possibility to restrict the analysis to only a narrow range of correlation times allows us to exclude the parts of the autocorrelation affected by undesirable processes from analysis and still obtain reliable results. For example, one may wish to ignore the early part of the correlation when the effects of the dye photophysics (triplet transitions [25]) or chemical reactions (protonation/deprotonation of fluorescent proteins [32, 33], photoisomerization [34]) become apparent, or simply when the noise at the short lag times is too high. On the other hand, the tail of the

#153144 - $15.00 USD Received 18 Aug 2011; revised 29 Sep 2011; accepted 1 Oct 2011; published 22 Nov 2011

autocorrelation may become affected by slow fluctuations, such as slow sample drifts or slow dye depletion due to photobleaching within a confined region [35]. The restriction of the fitting range in such situations may be preferable to including the processes other than diffusion into the fitting model, and in doing so increasing the number of variable parameters.

In the following section we show two examples of long-range fluctuations that can often be encountered in practice, where sFCS yields correct diffusion coefficients while the standard FCS measurements are difficult to interpret.

4.3. Robustness to slow axial drift

Slow axial drift of the membrane relative to the focal plane during the measurement can lead to two effects: First, the average fluorescence intensity changes as the membrane passes through the center of the measurement volume towards its upper or lower side. This usually becomes apparent in the autocorrelation as additional decay or rise at long times and as an overall offset. Second, the measurement volume a determined by the cross-section of the membrane and the focal plane continuously changes (Fig. 1(A)), influencing in a corresponding way also the diffusion time and the average number of molecules in the volume.

While the influence of the first effect on the fit results may be eliminated by excluding the long-time part of the autocorrelation from the fit, as shown in the previous section, the change of a during the measurement influences the autocorrelation at all lag times τ, and therefore requires more attention. We note that in standard FCS the change of a during the measurement renders any previous calibration of a, if possible at all, invalid, making a subsequent conversion of the diffusion time τ_D into the diffusion coefficient D using Eq. (5) highly inaccurate.

In order to investigate the effects of slow axial drift in sFCS, we first generated autocorrelation curves with the volume size a varying uniformly in the range $(a_0, a_0 + \Delta a)$ mimicking the volume change during the drift. Then, we added noise, and fitted the curves to Eq. (4). A series of curves with different Δa was generated. As the smallest value of a we chose 0.12 μm and the range width Δa was varied from 0, corresponding to a fixed position, to 0.28 μm, representing the largest drift.

The main result of these calculations, summarized in Fig. 5(A), is that the axial drift has a minimal effect on the diffusion coefficient obtained from the fit. The diffusion coefficient increased slightly with Δa, but the deviation from the true value remained below 3%. The single value of the volume size a obtained from fitting lies not far from the center of the interval $(a_0, a_0 + \Delta a)$, as might be expected. The relative concentration c, calculated from the fitted autocorrelation amplitude $g(0)$ and a, also increased with Δa, deviating by 10% from the true value at the largest Δa. The fit quality decreased for broader drift ranges, and the relative deviations of D and c depended somewhat on the chosen fitting range, however, not exceeding 6% for D and 45% for c in the worst case. While the diffusion coefficient determined with sFCS is minimally sensitive to the axial drift, the concentration is more strongly affected.

The effective diffusion time, calculated from the D and a values shown in Fig. 5(A), increases with Δa by a factor of up to three. Analogous calculations without scanning revealed a similar increase of τ_D. If a constant a is assumed, these large variations of τ_D with different drift ranges Δa translate into a variations of D also by a factor of three, a stark contrast to several per cent in sFCS.

In order to experimentally test the robustness of sFCS to axial drift revealed by these calculations, we performed sFCS measurements while moving the SLB (DOPC with Bodipy-Chol) uniformly through the measurement volume. The axial range covered during the measurement time of 100 s was Δz=1.8 μm. The autocorrelations measured both with and without circular scanning exhibit a large offset (Fig. 5(B)) and do not decay to a constant value at long lag times due to the slow changes in the mean fluorescence caused by the drift in and out of the

#153144 - $15.00 USD Received 18 Aug 2011; revised 29 Sep 2011; accepted 1 Oct 2011; published 22 Nov 2011

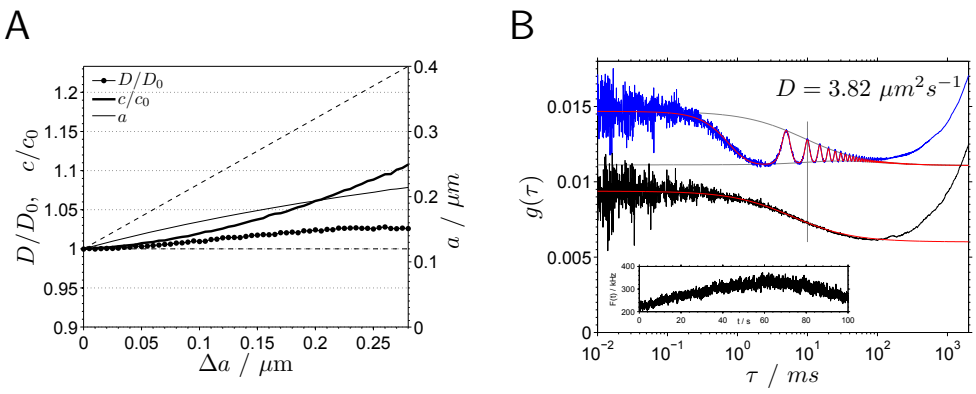

Fig. 5. A slow axial drift has a minimal effect on the sFCS results. A: relative diffusion coefficients D/D_0, relative concentrations c/c_0, and volume sizes a obtained from fits of simulated data; where the actual volume size parameter a continuously varied in the range $(0.12, 0.12+\Delta a)\,\mu$m. The model parameters: $D = 5\,\mu\text{m}^2\text{s}^{-1}$, $a_0 = 0.12\,\mu$m, $f = 200$ Hz, $R = 0.4\,\mu$m. The dashed lines indicate the range of volume sizes a covered by a given value Δa. B: Experimental autocorrelation curves with (blue) and without (black) circular scanning, where the objective focal plane was moved during the measurement uniformly along the optical axis by 1.8 μm, passing through the membrane. Both curves were fit in the range (0.01, 10) ms. The curve obtained without scanning was shifted down by $\Delta g(0) = 0.004$ for clarity. The inset shows the fluorescence intensity $F(t)$ during the measurement.

focal plane (Fig. 5(B), inset). Nevertheless, the fit to the initial part of the sFCS autocorrelation returns the correct diffusion coefficient $D = 3.8\mu\text{m}^2\text{s}^{-1}$. If the value of a from the sFCS fit is used to calculate the diffusion coefficient from the fit to the standard FCS data, a too high value of $D = 5.7\mu\text{m}^2\text{s}^{-1}$ is obtained.

These calculations and experiments show that slow drifts that change the size of the measurement volume, as well as the average fluorescence, on the time scales much slower than diffusion times, practically do not affect the diffusion coefficients obtained from fitting. The sFCS method is therefore robust to slow drifts.

4.4. Robustness to membrane fluctuations

Free-standing membranes in model systems, such as GUVs or flat membranes formed across apertures, as well as cell membranes, can exhibit thermal fluctuations on the time scales approaching those of diffusion [11, 36, 37]. The amplitude and time-scale of these fluctuations depends on the membrane tension, bending rigidity and the parameters of the surrounding medium. The presence of any structures providing support, for example, the cytoskeleton in cells, may efficiently dampen or suppress the membrane fluctuations.

In order to investigate how the fast axial fluctuations affect the sFCS measurements, we used a steady SLB and mimicked the membrane fluctuations by moving the objective axially with respect to the SLB by an objective piezo scanner. The objective scanner was programmed to perform a random walk in a potential centered around the membrane plane. The choice of the axial range within which the objective moved, the average step size and the time per step allowed us to control the amplitude and time-scale of the fluctuations.

Figure 6(A) compares the autocorrelations without and with the axial fluctuations, measured without circular scanning. The axial fluctuations are reflected in the autocorrelation as an ad-

#153144 - $15.00 USD Received 18 Aug 2011; revised 29 Sep 2011; accepted 1 Oct 2011; published 22 Nov 2011

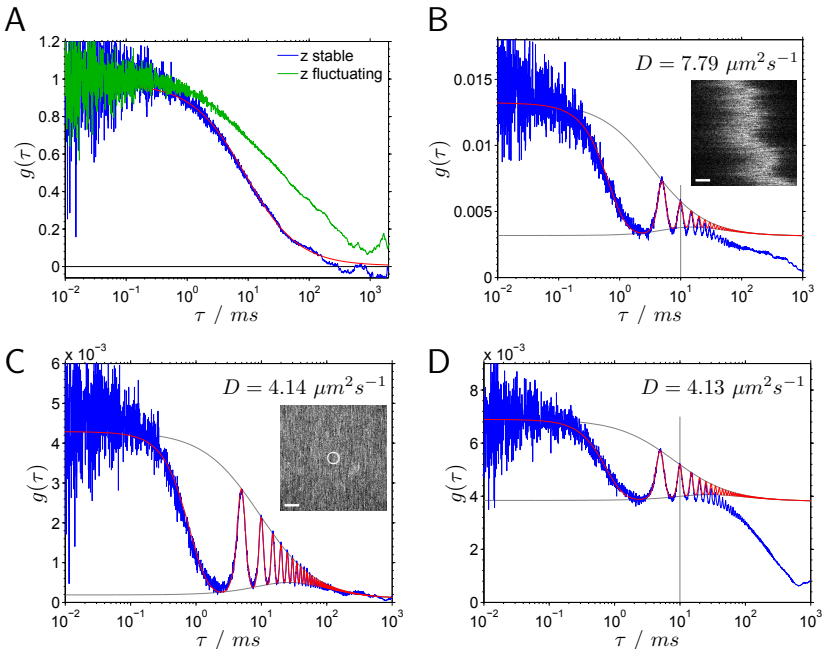

Fig. 6. The effect of membrane fluctuations on the sFCS results. Without circular scanning (A), and in the presence of axial fluctuations the autocorrelation curve (green) deviates significantly from the curve measured in the absence of axial fluctuations (blue), and cannot be described by a simple diffusion model. With circular scanning (C and D), the autocorrelation with axial fluctuations (D) still deviates from that without fluctuations (C), however, a fit of the initial part of the curve in the interval (0.01, 10) ms yields the same diffusion coefficient as obtained when the fluctuations are absent. The inset in C: SLB with the circular scan path. B: A measurement performed on the top pole of a fluctuating GUV with a fit of the initial part of the curve yields the expected diffusion coefficient (DOPC with DiO). The inset shows the GUV fluctuations (scale bars: 1 μm).

ditional correlation feature at longer times, making it difficult to fit the data and to reliably determine the diffusion time, and therefore the diffusion coefficient.

Since the axial fluctuations affect the correlation predominantly at longer times, we analyzed the sFCS autocorrelation curves at shorter correlation times, where the interference of the membrane fluctuations is expected to be minimal. Fitting the curves in the range 0.01–10 ms gives identical diffusion coefficients in absence and presence of axial fluctuations, as shown in Fig. 6(C–D). This demonstrates that sFCS is robust to the effects of membrane fluctuations on the correlation experiments.

The condition for this robust property of sFCS is that there is a range of correlation times where the fluctuations due to diffusion dominate, and where the fluctuations due to other effects can be neglected. This is the case of thermal fluctuations in membranes. The fluctuations in GUVs can be decomposed into modes with distinct amplitudes and relaxation times [38]. The mode amplitude and the relaxation time decreases with the mode number, therefore the effect of the thermal fluctuations at short correlation times, corresponding to short relaxation times of membrane fluctuations, is lower.

To test the sFCS performance on a membrane exhibiting thermal fluctuations, we prepared

#153144 - $15.00 USD Received 18 Aug 2011; revised 29 Sep 2011; accepted 1 Oct 2011; published 22 Nov 2011

GUVs that were not tensed by the osmolarity difference of the inside and outside solutions. These GUVs were fluctuating, as shown in the inset of Fig. 6(B), where the objective focus was positioned few μm below the top pole of the vesicle. The sFCS autocorrelation reflects these fluctuations as an additional correlation decrease in the range of hundred of ms, and an offset. Limiting the fit of the sFCS curve to the lag times below 10 ms yields the correct diffusion coefficient, as it did in the case of the artificially driven objective oscillations described above.

5. Discussion and conclusion

The presented circular sFCS applied to membranes is shown to posses two major advantages compared to standard FCS, both particularly important from the point of practical applications. First, the size of the measurement area need not be known for analysis, meaning that the results are not sensitive to the positioning of the membrane with respect to the focus. Second, the method is robust to disturbances occurring on time scales other than diffusion, since the analysis of the autocorrelation can be safely restricted to a narrow interval of correlation times.

The implementation of sFCS in this work is based on a single modification of a basic FCS setup: replacement of a fixed mirror by a mirror mounted on a scanner. A simple upgrade of an existing FCS instrument is therefore straightforward, without an increase in complexity required for other advanced FCS methods exploiting the benefits of spatio-temporal correlation, for example, the use of pulsed excitation or additional light polarization control [14, 39]. The method does not require any synchronization between excitation and detection, therefore the raw data processing is straightforward as in standard FCS. The autocorrelation is directly calculated using existing algorithms, no pre-sorting or aligning of the data, as in line scan methods, is necessary.

Another way to implement circular sFCS is, as shown previously [19, 20, 40], to include the option of a circular scan in an existing confocal laser scanning microscope with FCS capability. This requires only a software modification, as the optical and detection part is identical to a standard FCS, and the galvo scanners typically employed in home-built or commercial confocal scanning microscopes are capable of scanning along the required circular path.

As the technique differs from standard FCS only by addition of the circular motion, the usual performance indicators are not affected. In particular, the molecular brightness, in terms of photon counts per molecule per second, which determines the signal-to-noise ratio, remains the same as without scanning. The necessary measurement times stay in the range from tens of seconds to a few minutes; here 100 s were used for all presented results.

The particular piezo scanner used here is approximately 5 times slower than commonly used galvo scanners [20], with its frequency range limited to several hundreds of Hz. This sets a practical upper limit on the diffusion coefficient that can be measured to around $100\,\mu\mathrm{m}^2\mathrm{s}^{-1}$. This is fully sufficient for diffusion in phospholipid membranes, or for bulk 3D diffusion of molecules as small as GFP. The range of diffusion coefficients of several hundred $\mu\mathrm{m}^2\mathrm{s}^{-1}$, characteristic for smaller molecules in bulk aqueous solution, can be reached with laser scanning microscopes, where the galvo scanners can operate at kHz frequencies.

Since the scanning radius is smaller than $0.4\,\mu$m, the measurement is performed within a very small sample area. With the volume size with the parameter a equal to or larger than 0.15 μm, the detected fluorescence in standard FCS originates predominantly from within a circle of radius $3a = 0.45\,\mu$m. With scanning FCS as used here, the probed area is larger only by a factor of approximately 4 (radius of approx. $0.85\,\mu$m). It is therefore not necessary to have a sample with a large flat homogeneous region to scan over as in other sFCS methods, or FRAP experiments. This is important for potential applications on membranes with small domains of different phases or composition, or measurements on cellular surfaces, where it may be difficult to find a large area of horizontal homogeneous membrane. Domains smaller than the laser spot

#153144 - $15.00 USD Received 18 Aug 2011; revised 29 Sep 2011; accepted 1 Oct 2011; published 22 Nov 2011

(lipid rafts) are averaged over in the same way in both standard and scanning FCS. In order to gain access to smaller spatial scales, where the presence of sub-resolution lipid domains could be detected, combination of the presented method with superresolution FCS (STED-FCS [41]) could be considered. This would require reduction of the scanning radius by the same factor by which the measurement volume size is reduced, leading to a scanned area larger than the static measurement volume by a similar factor (~ 4) as in the presented implementation.

An attractive possibility is the direct extension of sFCS to two colour cross-correlation measurements on surfaces, a method that allows the quantification of binding interactions between molecules labeled with different dyes [8, 9]. An important benefit of sFCS would be the knowledge of the size of both measurement volumes a_1 and a_2, which are in general different due to their dependence on wavelength. Of interest is usually the fraction f_2 of interacting molecules: $f_2 = c_{12}/(c_2 + c_{12})$, where c_1, c_2, c_{12} are the concentrations of species with either of the two or both labels. It can be determined from the experimental ratio of the cross-correlation $g_{12}(0)$ and autocorrelation $g_i(0) = 1/(4\pi a_i^2(c_i + c_{12}))$ amplitudes, taking into account the different sizes a_1 and a_2 of the two concentric areas/volumes (Eq. (7)):

$$\frac{g_{12}(0)}{g_1(0)} = \frac{2a_1^2}{a_1^2 + a_2^2} \frac{c_{12}}{c_2 + c_{12}} \tag{7}$$

The knowledge of a_1 and a_2 would then allow us to avoid the usually made assumption that $a_1 = a_2$ [35], and to accommodate the different volume sizes in the interpretation of the auto- and cross- correlation amplitudes [8], leading to better quantitative estimates of the interacting fraction of molecules.

The circular sFCS method is also applicable to diffusion measurements in three dimensions, as shown previously with a laser scanning microscope using two-photon excitation [20]. Here, a careful attention must be paid to using an appropriate model for the measurement volume and therefore the autocorrelation function, as the simple 3D gaussian model is not sufficiently accurate to describe the combined effects of excitation beam and detection pinhole in spatio-temporal correlation experiments [14].

The simplicity of the presented method compared to other spatio-temporal fluorescence correlation techniques, and its robustness to various disturbing effects makes it particularly suitable for quantitative characterization of dynamical behaviour and interactions of molecules in membranes and other planar systems.

Acknowledgements

We would like to thank Jens Ehrig, Christoph Herold and Le Mu for assistance with the sample preparation. This work was supported by the EU (FP7-216027).

#153144 - $15.00 USD Received 18 Aug 2011; revised 29 Sep 2011; accepted 1 Oct 2011; published 22 Nov 2011